Semiconductor Physics, Quantum Electronics & Optoelectronics, 2025. V. 28, No 4. P. 400-412.

Semiconductor physics

X-band microwave properties of polyvinyl chloride/oxidized activated carbon thin-film composites

L.M. Grishchenko[1,2,3], V.E. Diyuk[1,2], D.O. Zhytnyk[4], I.P. Matushko[5], Yu.V. Noskov[6], N.S. Novychenko[7], R.T. Mariychuk[8], O.Yu. Boldyrieva[1], M.V. Makarets[5], V.V. Klepko[9], O.V. Mischanchuk[3], V.V. Lisnyak[3,9,10*]

[1]*Faculty of Chemistry, Taras Shevchenko National University of Kyiv, 64/13, Volodymyrska Street, 01601 Kyiv, Ukraine*
[2]*Institute of Engineering Thermophysics, NAS of Ukraine, 2a, Marii Kapnist Street, 03057 Kyiv, Ukraine*
[3]*Chuiko Institute of Surface Chemistry, NAS of Ukraine, 17, Oleha Mudraka Street, Kyiv 03164, Ukraine*
[4]*Faculty of Radiophysics, Electronics and Computer Systems, Taras Shevchenko National University of Kyiv, 4g, Hlushkova Avenue, 03022 Kyiv, Ukraine*
[5]*Faculty of Physics, Taras Shevchenko National University of Kyiv, 4g, Hlushkova Avenue, 03022 Kyiv, Ukraine*
[6]*V. Kukhar Institute of Bioorganic Chemistry and Petrochemistry, NAS of Ukraine, 50, Kharkivske Shose, 02155 Kyiv, Ukraine*
[7]*Department of Electron-Probe Research of Multifunctional Materials, Technical Center of the National Academy of Sciences of Ukraine, 13, Pokrovska Street, 04070 Kyiv, Ukraine*
[8]*Department of Ecology, Faculty of Humanities and Natural Science, University of Presov, 17th November Street 1, 08001 Presov, Slovak Republic*
[9]*Institute of Macromolecular Chemistry, NAS of Ukraine, 48, Kharkivske Shose, Kyiv 02155, Ukraine*
[10]*Western Caspian University, 31, Istiglaliyyat Street, AZ 1001 Baku, Republic of Azerbaijan*
[*]*Corresponding author e-mail: lisnyak@nas.gov.ua*

Abstract. Poly(vinyl chloride) (PVC) and oxidized activated carbon (AC-H_2O_2) powders were hot-pressed into thin-film composites (TFCs) with a composition of $(PVC)_{100-x}/(AC\text{-}H_2O_2)_x$, where x = 0.2…30 wt.%. We investigated the nanostructure, morphology, and composition of the AC-H_2O_2 filler using scanning electron microscopy and energy dispersive X-ray spectroscopy. Thermal analysis methods were employed to evaluate the thermal stability of the surface carbon-oxygen groups of the AC-H_2O_2 filler. The effect of AC-H_2O_2 filler content on the electromagnetic transparency of the $(PVC)_{100-x}/(AC\text{-}H_2O_2)_x$ TFCs was evaluated at X-band microwave frequencies. Microwave transmission showed only a weak dependence on the filler concentration. However, reflection losses varied from –21.7 to –11.8 dB as x increased from 0.2 to 30 wt.%. Comparing analogous composites containing initial AC revealed that filler oxidation significantly affects performance. The difference in the average reflection loss between $(PVC)_{100-x}/(AC\text{-}H_2O_2)_x$ and $(PVC)_{100-x}/(AC)_x$ TFCs ranged from –3.4 dB at x < 5 wt.% to –8.7 dB at x < 20–30%.

Keywords: thin-film composites, poly(vinyl chloride), activated carbon, oxidation, electromagnetic shielding, microwave reflection.

https://doi.org/10.15407/spqeo28.04.400
PACS 62.23.Pq, 65.80.-g, 68.55.-a, 74.78.Na, 81.05.Rm, 81.05.U-, 81.05.Zx

Manuscript received 25.02.25; revised version received 04.10.25; accepted for publication 26.11.25; published online 15.12.25.

1. Introduction

The rapid advances in electronics in recent years have given rise to significant concern: the emergence of unwanted electromagnetic radiation (EMR), which has the potential to interfere with the proper functioning of electronic equipment and various devices [1, 2]. This EMR has also been found to be detrimental to the health of living organisms [3, 4]. The proliferation of electronic devices is increasing continuously, and this trend will continue in the future. In response to this growing concern, scientists have initiated efforts to develop materials capable of shielding EMR [5, 6]. Conventionally, metals have been used for shielding applications; however, this has resulted in secondary EMR contamination due to wave reflection from the metal. Therefore, there is an urgent need to explore shielding materials (SMs) whose action is based on absorption of microwaves to minimize EMR contamination [7, 8]. SMs with properties such as lightness, low thickness, high flexibility, and broadband absorption are promising in this regard [9, 10]. Common SMs are carbon compounds and metals incorporated into

the polymer matrix [11, 12]. Achieving maximum microwave absorption efficiency requires the dispersion of different types of fillers with varying concentrations in the polymer matrix and the use of various composite thicknesses [13–16].

Polymer-based composites are of particular interest among the SMs, and it is advisable to use polymers that can not only perform the function of an inert matrix for the introduction of various fillers but also can chemically interact with them, performing several functions, namely stabilizing the near-zero valence state of the filler distributed in it, preventing the filler oxidation, *etc*. [17]. These advantages of polymers make the scope of their application extremely wide, ranging from biomedical applications to stealth technologies [18, 19]. The practical implementation of metal-based SMs is hindered by several significant limitations, including high density, low corrosion resistance, and significant processing costs [20]. These limitations preclude the application of metal-based SMs in cases when EMR absorption is extremely high [21]. In contrast, carbon materials (CMs) possess distinctive mechanical properties resulting from the carbonization of hard carbonaceous structures and physicochemical properties tunable by variations in their surface chemistry. Besides, CMs are characterized by a developed porous structure with high thermal stability and the ability to be tuned physically and chemically [22]. The CMs showed a variety of essential properties, including low density. They can have excellent conductivity and superior mechanical strength and can be prepared from raw low-cost materials of natural origin [23, 24]. The applications of CMs are extensive, including catalysts, adsorbents, supercapacitors, and fillers in composites for EMR shielding [25–28]. In addition, CMs have the potential to replace polymers in medical nanocontainers [29]. The porosity of carbon structures makes them good candidates for using various fillers and modifiers, allowing for multifunctional applications [30, 31]. The prospect of obtaining porous CMs from natural sources is particularly encouraging, as natural lignin/cellulose are both inexpensive and can be produced from naturally renewable resources. Natural carbonaceous biomaterials possess a significant number of surface functional groups as well as small pores and channels that can be preserved under certain conditions during their preparation [32, 33]. Additionally, CMs derived from raw carbonaceous biomaterials are usually capable of chemical modification, which is important for surface tailoring and functionalization to obtain a functionalized surface with a set of predetermined properties, since the introduction of functional groups or heteroatoms into the carbon surface layer can significantly affect not only the chemical properties of these materials [34–36], but also the nature of the material interaction with EMR [37–39].

This work aimed to obtain composite material based on a polymer matrix and oxidative modified activated carbon (AC) and to study the microwave properties of the obtained composites.

2. Experimental

2.1. Materials

Hydrogen peroxide (H_2O_2, 35%), hydrogen chloride (HCl, 30%+), polyvinyl chloride (PVC, 99.89%), and other reactants were purchased from Sigma-Aldrich. Double-distilled water (DDW) from a water bi-distiller was used for washing and dilution procedures. Di-butyl phthalate (DBP, 99.89%+) plasticizer was supported by Yuanyuci Co. (China). To prepare the required 3 v/v% HCl and 10 v/v% H_2O_2 water solutions, more concentrated reagents were diluted with 18 MOhm·cm deionized DDW prepared with the Master-Q series deionized water system.

The carbonaceous bio-source, *Prunus armeniaca* L. stones, was collected, dried, and used for the preparation of AC by carbonization/steam activation [25]. First, the AC powder was deashed by repeated washing with HCl solution (3 v/v%) and then with DDW to neutralize acid residues. The AC fraction within 0.5…1.1 mm was separated for future studies. Oxidative modification was performed by treating the deashed AC powder with 10 (v/v)% H_2O_2 solution to produce AC-H_2O_2. The treatment was performed by immersing 1 g of AC powder in 100 mL of 10 (v/v)% H_2O_2 solution in a glass for 4 h, when the resulting AC-H_2O_2 solid was filtered through the filtration paper in a Büchner funnel, washed repeatedly with DDW to a neutral pH of washing waters, and then collected and dried in air at 120 °C.

2.2. Preparation

PVC/AC-H_2O_2 thin film composites (TFCs) were prepared as follows. A series of $(PVC)_{100-x}/(AC\text{-}H_2O_2)_x$ TFCs were hot pressed from the powders of PVC and AC or AC-H_2O_2, where AC was taken in various weight ratios to PVC, x = 0.2…30 wt.% of AC or AC-H_2O_2. In the typical preparation, the deashed AC or AC-H_2O_2 powder was first ground in an agate mortar. Then 0.2 g of PVC powder was mixed with the required weighted mass of AC or AC-H_2O_2. This mixture was ground again in the same mortar to homogenize and then poured into a mold on a (poly)amide substrate, and 70 mg of DBP was added to plasticize the PVC. The $(PVC)_{100-x}/(AC\text{-}H_2O_2)_x$ TFCs or $(PVC)_{100-x}/(AC)_x$ TFCs were pressed at a pressure of 10 MPa and a temperature of 175 °C for 1 min. The same procedure, without the carbon filler, was used to prepare PVC thin films (TFs). The samples of $(PVC)_{100-x}/(AC\text{-}H_2O_2)_x$ TFCs, $(PVC)_{100-x}/(AC)_x$ TFCs, and PVC TFs were approximately 23×10×0.25 mm and were used for further tests as in [40–43].

2.3. Characterization

Thermogravimetric analysis (TGA) of AC and AC-H_2O_2 fillers was performed using a Q-1500 D thermal analysis instrument in the configuration designed by F. Paulik, J. Paulik, and L. Erdey. The TGA was performed in an air atmosphere, with a heating rate of 14°C·min^{-1}, within 20…900 °C [41]. Additionally, the AC and AC-H_2O_2 fillers were investigated by temperature-programmed desorption mass spectrometry (TPD MS) in vacuum [25].

The surface morphology of the samples was visualized by scanning electron microscopy (SEM) using a Tescan Mira 3 LMU microscope [34, 36, 39]. Energy dispersive X-ray (EDX) microanalysis was carried out on an INCA Energy 450 XMax 80 microanalysis system from Oxford Instruments mounted on the microscope.

The water sorption test was carried out by measuring the weight loss after adsorption of water moisture on each filler powder by a standardized desiccator method. The nitrogen adsorption-desorption porosimeter was used to determine the porosity of AC and AC-H_2O_2, measuring the Brunauer–Emmett–Teller (BET) surface area S_{BET} and the total pore volume V_S. The types of oxygen-containing groups were determined by the Boehm titration [41]. Fourier transform infrared (FTIR) spectra for the $(PVC)_{100-x}/(AC\text{-}H_2O_2)_x$ TFCs were recorded using a Nicolet iS50 FTIR spectrometer. The carbon surface chemistry was investigated using attenuated total reflection (ATR) FTIR spectroscopy on a Shimadzu Prestige 21 instrument, which was equipped with a PIKE single reflection ATR accessory and a ZnSe ATR crystal. For the carbon fillers, 1,000 scans were collected with a scan step of 2 cm^{-1}, and the ATR spectra were normalized by applying atmospheric and spectral corrections. Finally, the microwave reflection loss (S_{11}) and microwave transmission loss (S_{21}) of the $(PVC)_{100-x}/(AC\text{-}H_2O_2)_x$ TFCs and PVC TFs were measured in the X-band as in [44, 45]. Optical micro photos of $(PVC)_{100-x}/(AC\text{-}H_2O_2)_x$ TFCs were captured with a Zeiss LSM 800 confocal microscope.

3. Results and discussion

3.1. SEM and SEM-EDX

In Figs 1a and 1b, the surface of the apricot stone is covered with micrometer-sized, irregularly shaped, large craters and pits, with some areas appearing darker and more irregular. The surface is rough and uneven, with small bumps and ridges scattered throughout. The surface has been sputtered with gold to prevent charge collection on the non-conductive sample surface, and the energy-dispersive characteristics X-ray fluorescence is clearly visible in the EDX spectra, describing the elemental composition of the sample (see, for example, Fig. 1c).

As demonstrated in Table 1, the results of the SEM-EDX microanalysis indicated that the carbonization of apricot stones resulted in a reduction in oxygen and an increase in carbon concentration within the analyzed solid. Conversely, the oxidation of the resulting AC exhibited the opposite effect, with an increase in oxygen and a decrease in carbon.

3.2. Texture and surface chemistry studies

The size of AC particles was within 0.5…1.1 mm. The water absorption capacity of AC powder was 0.42 $cc\cdot g^{-1}$, and the specific BET surface area of AC was 930 $m^2\cdot g^{-1}$, and the total pore volume V_S was 0.512 $cm^3\cdot g^{-1}$. From the adsorption data, AC-H_2O_2 has an S_{BET} of 850 $m^2\cdot g^{-1}$ and V_S is 0.488 $cm^3\cdot g^{-1}$. According to the Boehm titration, the 2.8 and 9.5 at.% of oxygen heteroatoms are in the carboxyl groups of 0.21 and 0.28 $mmol\cdot g^{-1}$, in the anhydride/lactone groups of 0.1 and 0.26 $mmol\cdot g^{-1}$, and in the phenol groups of 0.30 and 0.52 $mmol\cdot g^{-1}$, respectively.

3.3. TGA

Fig. 4 shows the TGA results of the initial AC sample and the AC-H_2O_2 sample prepared by oxidation of AC with H_2O_2.

Thermograms (1) and (3) show that the thermal decomposition of the samples is quite similar and has a gradual character. It is obvious that both samples contain a significant amount of adsorbed water, as evidenced by a sharp weight loss under heating from 30 to 114 °C [46, 47]. At the same time, the AC sample contains less adsorbed water, as it loses less weight within this temperature range, with a difference of 2 wt.% (9.5 *vs* 11.5 wt.%). With further heating above 120 °C, the weight loss of AC-H_2O_2 is small, close to 6%, and it has an almost a linear trend up to a temperature of 534 °C (see thermogram 3 in Fig. 4). This weight loss is most likely due to the cleavage of non-thermally stable oxygen-containing groups, namely carboxyl, anhydride, and lactone groups [47]. Upon heating up to 534 °C, the AC exhibits better thermal stability than AC-H_2O_2, showing a slightly lower weight loss effect of ~3.5%, due to the lower concentration of surface oxygen-containing groups in the AC sample.

At temperatures above 534°C, both samples show an intense weight loss due to the combustion of carbon in the presence of atmospheric oxygen. At the same time, up to 770 °C, the AC-H_2O_2 sample is more thermally stable than the unmodified AC sample. This is also clearly seen in the DTG data (thermograms 2 and 4). Particularly, they show that the peak of the most intense burnout of the AC sample is centered at 640 °C, while for the oxidized AC, this peak is shifted by 20 °C to a higher temperature (660 °C). The higher thermal stability of the AC-H_2O_2 sample compared to the AC sample can be explained by two factors. Firstly, the oxidation of AC by H_2O_2 leads to the formation of phenolic groups on the surface. These groups are quite thermally stable and

Table 1. Results of the SEM-EDX microanalysis of the apricot stones, initial AC, and oxidized AC-H_2O_2 samples.

EDX spectrum	Apricot stones		AC		AC-H_2O_2	
	Element content, at.%					
	C	O	C	O	C	O
Spectrum 1	71.24	28.76	97.14	2.86	86.39	13.61
Spectrum 2	73.84	26.16	97.25	2.75	94.64	5.36
Mean	72.54	27.46	97.20	2.80	90.51	9.49

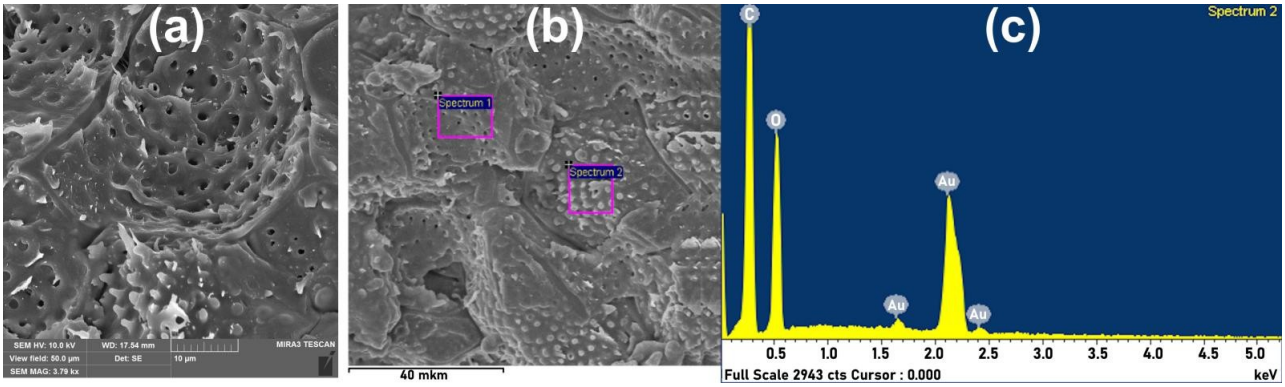

Fig. 1. (a) High-resolution SEM image of an apricot stone sample, (b) SEM image showing the area of EDX analysis, and (c) typical EDX spectrum obtained from the section (2) shown in (b).

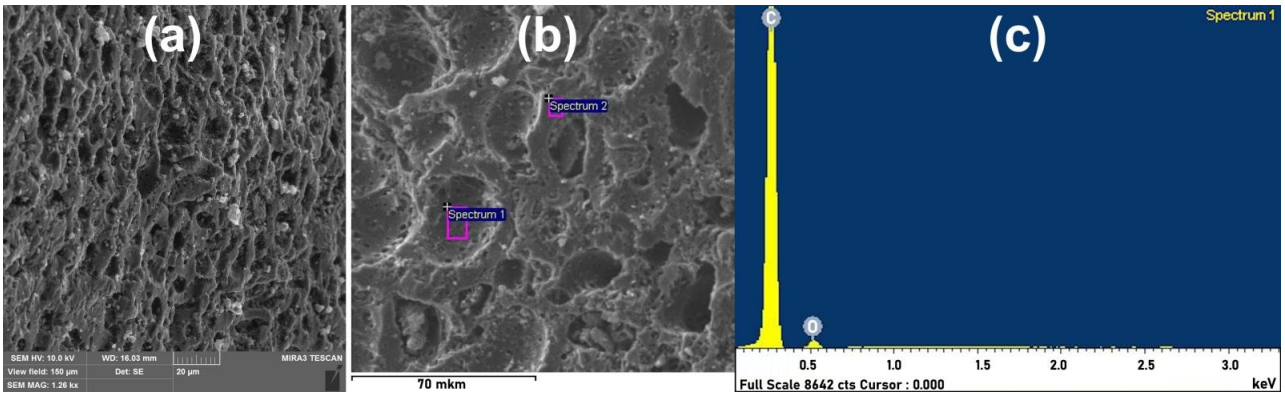

Fig. 2. (a) High-resolution SEM image of the AC sample, (b) SEM image of the AC sample showing the EDX analysis area, and (c) typical EDX spectrum obtained from the section of AC.

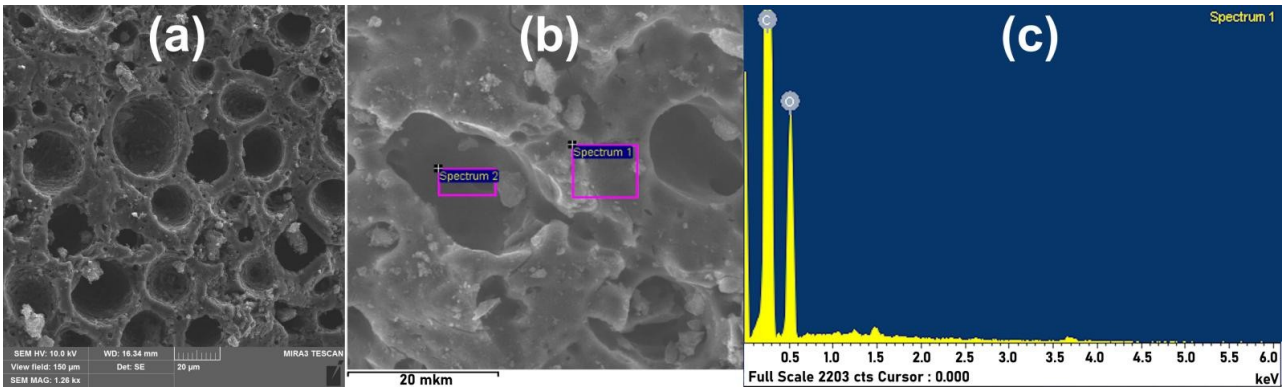

Fig. 3. (a) High-resolution SEM image of the AC-H_2O_2 sample, (b) SEM image of the AC-H_2O_2 sample showing the EDX analysis area, and (c) typical EDX spectrum obtained from the section of the AC-H_2O_2 sample.

decompose at temperatures above 650…700 °C. Secondly, oxidation results in the transformation/removal of the most chemically active areas of the AC surface, which can increase the thermal stability of the oxidized carbon surface. The complete combustion of both samples finishes at 870…890 °C.

3.4. FTIR ATR

Fig. 5 shows the FTIR ATR spectra of the AC and AC-H_2O_2 samples. The most intense absorption bands at 1517 and 1548 cm^{-1}, as well as others within 1600…1470 cm^{-1}, correspond to the skeletal vibrations of aromatic and/or conjugated C=C bonds.

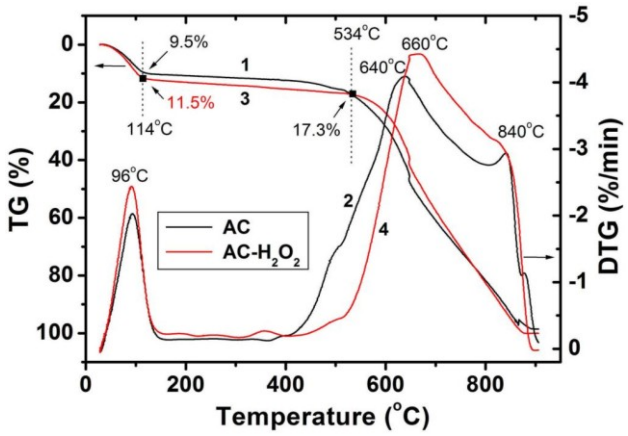

Fig. 4. Thermogravimetric (*1*, *3*) and differential thermogravimetric (*2*, *4*) thermograms of (*1*, *2*) AC and (*3*, *4*) AC-H_2O_2.

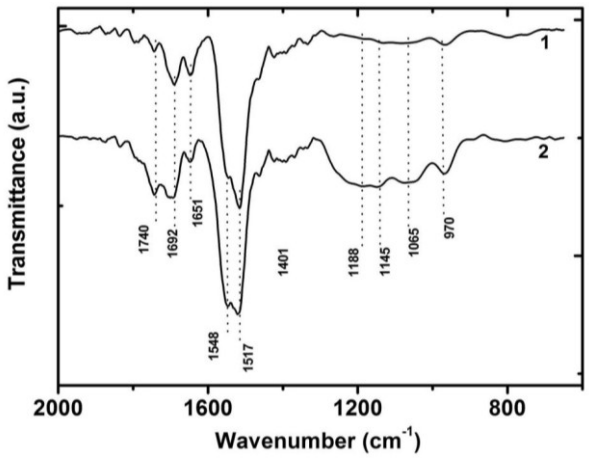

Fig. 5. FTIR ATR spectra of (1) AC and (2) AC-H_2O_2.

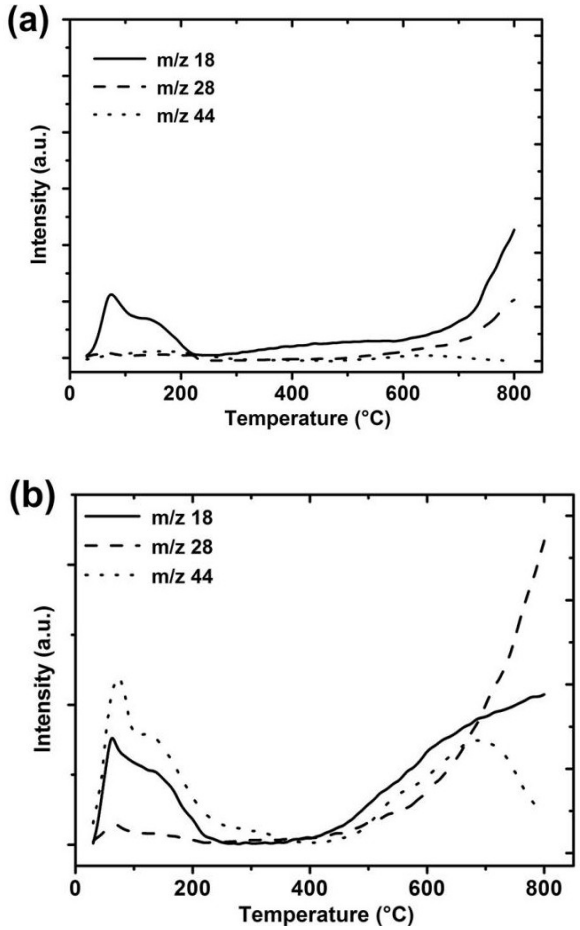

Fig. 6. Typical TPD MS profiles: (a) AC and (b) AC-H_2O_2.

The carbon matrix of AC consists mainly of sp^2-hybridized carbon atoms, which explains the significant absorption within this spectral range. Oxidation of AC with a 15% H_2O_2 water solution has a weak effect on the carbon surface and leads to insignificant changes in the intensity of the absorption bands of the carbon matrix. Presumably, during oxidation, a temporary heterogenization of the carbon surface layer of the AC occurs, and some carbon atoms can be removed or transferred to another state. The absorption bands at 1740, 1692, and 1651 cm^{-1} are attributed to vibrations of C=O bonds, which are part of the anhydride, lactone, carboxyl, and quinone groups of the AC. Oxidation of AC leads to a redistribution and a significant increase of absorption intensity within 1750…1650 cm^{-1} due to the formation of new C=O bonds. During oxidation, the content of carboxyl (1692 cm^{-1}), anhydride, and lactone (1740 cm^{-1}) groups demonstrates the greatest increase. Broad absorption bands at 1188 and 1145 cm^{-1} are associated with vibrations of C–OH phenolic groups. The increase in the absorption intensity is greatest within 1250…1090 cm^{-1}, indicating the preferable formation of phenolic groups due to oxidation of the AC surface. Quite intensive bands at 1065 and 970 cm^{-1} can be attributed to the absorption of C–O bonds, O–H groups of acids, or C–O–C groups of surface anhydrides and lactones. The increase in intensity of the absorption bands at 1640…1750 and 1400…950 cm^{-1} is caused by a significant increase in oxygen content in the oxidized AC sample compared to the untreated AC.

3.5. TPD MS

The intensive signals of molecular ions with m/z 18 (H_2O^+), m/z 28 (CO^+), and m/z 44 (CO_2^+) are observed in the TPD-MS spectra of the AC and AC-H_2O_2 in vacuum.

The AC sample adsorbs H_2O and CO_2, and both physisorbed can be readily removed within the temperature range of 30…100 °C (Fig. 6a). Within the range 100…300 °C, water is bound to polar surface groups and/or adsorbed in AC micropores. Within the same temperature range, the decomposition of a few carboxyl groups is observed, resulting in the release of CO_2. At temperatures exceeding 500 °C, a pronounced release of CO and water occurs, which are byproducts of the thermal decomposition of phenolic groups. A slight release of

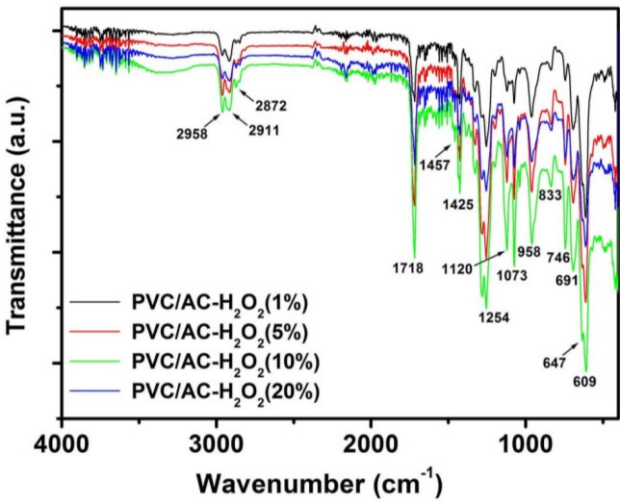

Fig. 7. FTIR spectra of $(PVC)_{100-x}/(AC\text{-}H_2O_2)_x$ TFCs where x = 1, 5, 10, and 20 wt.% of AC-H_2O_2.

CO_2 within 500…750 °C is attributable to the thermal decomposition of anhydride and lactone surface groups of AC.

For AC oxidized with H_2O_2, Fig. 6b shows the enhanced CO_2 release in the 30…300 °C range (m/z 44) that indicates the formation of carboxyl groups during oxidation, as also reflected in the functional group concentrations reported in Section 3.2. In addition to carboxylic groups, the oxidation of the AC surface leads to the formation of anhydride and lactone groups, as evidenced by a significant release of CO_2 within a wide temperature range of 500…800 °C. The presence of a significant amount of these groups indicates a high degree of oxidation of the AC surface by the H_2O_2 water solution, thereby enabling neighboring carboxyl or carboxyl and phenolic groups to interact with each other.

For the AC-H_2O_2 sample, surface decomposition is largely suppressed within 250–500 °C, as evidenced by the near-zero, plateau-like m/z intensities in Fig. 6b. This observation indicates that oxidation treatment with H_2O_2 water solution, in contrast to HNO_3 solution, does not involve all active centers of the AC surface. Formation of oxygen-containing groups occurs exclusively in the most active areas of the carbon matrix surface.

3.6. FTIR

In the spectra of $(PVC)_{100-x}/(AC\text{-}H_2O_2)_x$ TFCs, some characteristic bands of PVC can be seen (Fig. 7). The absorption bands were assigned as in [41]. Among the high-frequency bands, a peak at 2911 cm^{-1}, attributed to elastic C–H vibrations, is of particular importance. An intense narrow band at 1718 cm^{-1} indicates the presence of carbonyl (C=O) in PVC macromolecules, formed by dechlorination (oxidation) of the PVC polymer during its thermal compression. The band at 1425 cm^{-1} is associated with CH_2 deformation vibrations, and the strong doublet IR band with a maximum at 1254 cm^{-1} is due to CH–Cl out-of-plane angular deformation vibrations. The band with a maximum at 958 cm^{-1} is attributed to C–H out-of-plane trans-strain. The intense peak at 609 cm^{-1} is due to elastic vibrations of the C–Cl bond. Smaller peaks at 691 and 833 cm^{-1} are also related to the same bond. Some of the IR bands are due to the DBP present in the films. These are the bands at 1073, 1120, 2872, and 2958 cm^{-1}.

The characteristic bands of AC in the spectrum of the AC-H_2O_2 sample appear mainly in the short wavelength range, where the most intense PVC bands are found. As a result, it is not easy to distinguish the specific bands of AC because they are superposed with strong polymer bands. Typically, these carboxyl groups (C–O) are always present in the AC-based carbons and are part of carboxylic acids, aldehydes, lactones, ethers, and other functional groups on the carbon surface. These groups typically absorb within 1100…1450 cm^{-1}. However, the spectra of the films contain numerous intense characteristic peaks of PVC and DBP within the above spectral range. In the range 1500…1600 cm^{-1}, among several small peaks, some may be due to the polyaromatic C=C elastic vibrations of sp^2-hybridized carbon atoms in the carbon matrix of the AC-H_2O_2 sample. The characteristic bands of PVC in the FTIR spectra of the films, regardless of the concentration of AC-H_2O_2 present, usually show only slight shifts compared to the pure PVC polymer, or sometimes no shift at all. This indicates that there is no chemical interaction between PVC and AC-H_2O_2 in these TCFs. However, there may be physical interactions such as Van der Waals bonding.

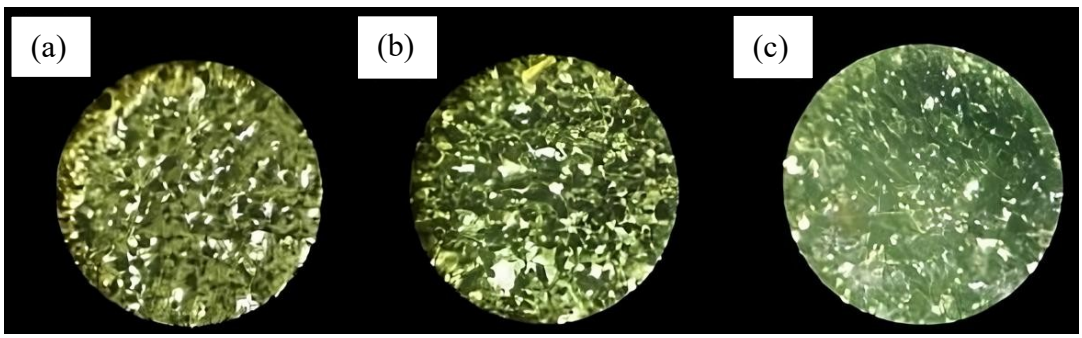

Fig. 8. (a-d) Optical photographs of $(PVC)_{100-x}/(AC\text{-}H_2O_2)_x$ TFCs, where x = 5 wt.% (a), 10 wt.% (b), and 30 wt.% (c) at 56× magnification.

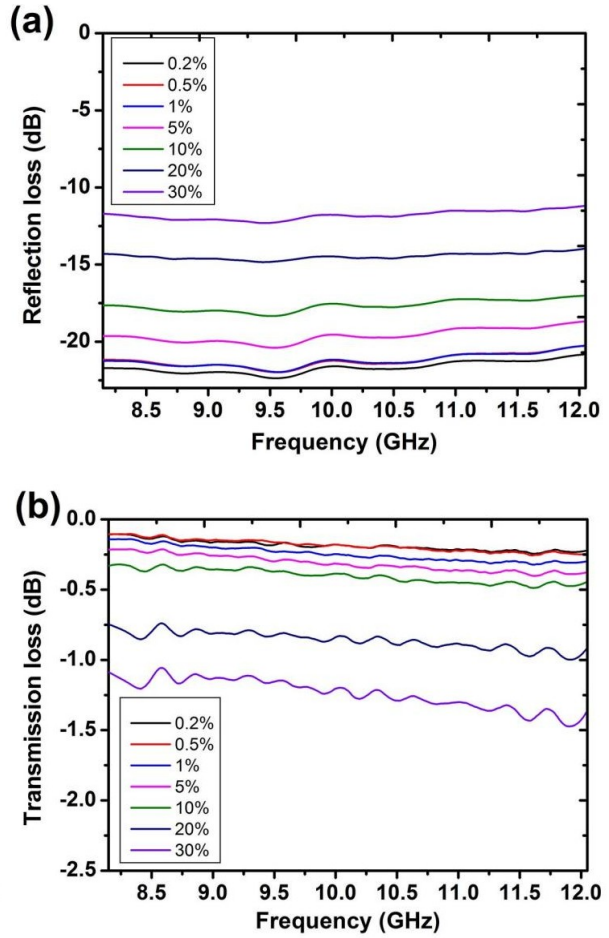

Fig. 9. Frequency dependences of (a) reflection loss and (b) transmission loss values of $(PVC)_{100-x}/(AC\text{-}H_2O_2)_x$ TFCs within the X-band.

Fig. 8 shows typical optical photographs of $(PVC)_{100-x}/(AC\text{-}H_2O_2)_x$ TFCs, and Figs. 9a and 9b present the X-band microwave properties.

A comparison of the reflection loss values within the X-band (see Table 2) reveals that the $(PVC)_{100-x}/(AC\text{-}H_2O_2)_x$ TFCs exhibit a measurable ability to reflect microwave radiation, at least within the range of the investigated $AC\text{-}H_2O_2$ filler concentrations. The $(PVC)_{70}/(AC\text{-}H_2O_2)_{30}$ TFCs, which contain the highest $AC\text{-}H_2O_2$ concentration, exhibited the highest mean reflection loss value of –11.8 dB. Additionally, it is worth noting that the difference between the minimum and maximum reflection loss values is close to 2 dB (see Table 2). Negative mean reflection loss values generally indicate that some portion of the incident wave was reflected. The more negative values, the more incident microwave energy is absorbed. More negative values correspond to higher absorption (*i.e.*, lower reflection), and *vice versa*.

According to the data, composites with lower filler content demonstrated more negative mean reflection loss values (*e.g.*, –21.7 dB), whereas higher filler concentrations resulted in less negative numeric values (*e.g.*, –11.8 dB).

With increasing concentration of carbon filler, the electrical conductivity of TFC increases. It can cause a mismatch in impedance between the material and free space (typically air), leading to a higher surface reflection and less wave penetration into the bulk, where effective absorption usually occurs. Additionally, high concentrations of $AC\text{-}H_2O_2$ filler in $(PVC)_{100-x}/(AC\text{-}H_2O_2)_x$ TFCs may cause agglomeration of the filler, which decreases dispersion uniformity and reduces dielectric losses. Other contributing factors include the saturation of conductive pathways, which limits further energy dissipation, and the reduced dipole mobility of the polar groups introduced during oxidation, which diminishes polarization-related losses. Consequently, $(PVC)_{100-x}/(AC\text{-}H_2O_2)_x$ TFCs can change the properties from being efficient microwave absorbers to primarily behaving as reflectors. This behavior is particularly pronounced when the TFC thickness is low and dielectric or magnetic loss mechanisms are insufficient to compensate for increased conductivity. Overall, the observed trend – where mean reflection loss values become less negative with increasing filler concentration – suggests that the composites become increasingly reflective rather than absorptive. It could be due to

Table 2. Microwave properties of $(PVC)_{100-x}/(AC\text{-}H_2O_2)_x$ TFC samples.

x, wt.%	Reflection loss, dB			Transmission loss, dB		
	Min	Mean	Max	Min	Mean	Max
0.0	–23.7	–22.8	–21.6	–0.1	–0.1	–0.1
0.2	–22.4	–21.7	–20.8	–0.2	–0.2	–0.1
0.5	–22.0	–21.2	–20.3	–0.3	–0.2	–0.1
1	–22.0	–21.2	–20.3	–0.3	–0.3	–0.1
5	–20.4	–19.6	–18.7	–0.4	–0.3	–0.2
10	–18.3	–17.7	–17.0	–0.5	–0.4	–0.3
20	–14.8	–14.5	–14.0	–1.0	–0.9	–0.7
30	–12.3	–11.8	–11.2	–1.5	–1.2	–1.1

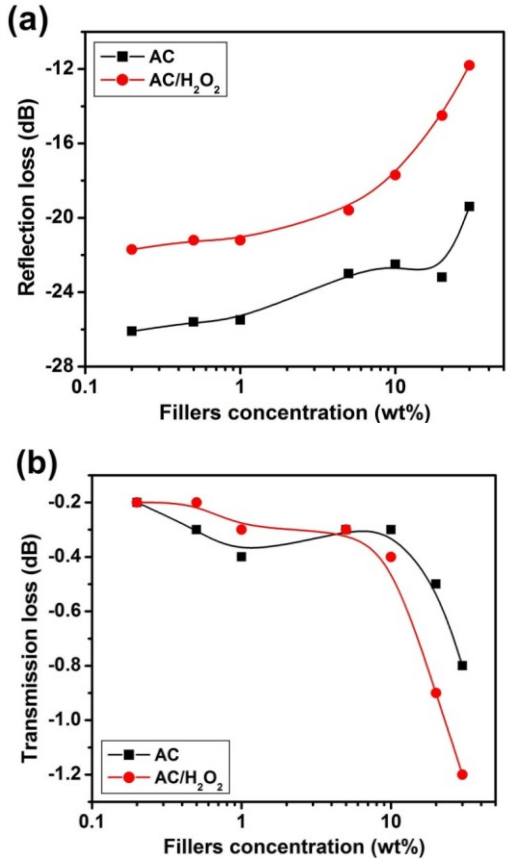

Fig. 10. Comparison of (a) the mean reflection loss and (b) the mean transmission loss for $(PVC)_{100-x}/(Filler)_x$ TFC samples, where the filler is either AC or AC-H_2O_2, within the X-band. The numeric values are plotted as a function of filler concentration (wt.%).

increased surface reflection caused by surface impedance mismatch and reduced internal energy dissipation mechanisms. Transmission loss typically describes the part of the incident power that was transmitted through a material. More negative transmission loss values indicate greater loss of the transmitted signal, meaning less energy passes through the material. As shown in Table 2, the transmission loss values become more negative (from –0.2 to –1.2 dB) with increasing AC-H_2O_2 filler concentration, indicating a decrease in transmitted microwave power. Note that the difference between the minimum, mean, and maximum transmission loss values is small.

Comparing transmission loss values within the X-band range, one can ascertain that the data reveal the well-known tendency for transmission loss values to decrease with increasing carbon filler concentration in conditionally radio-transparent PVC. However, since the samples are TFCs, further studies with larger samples and the calculations of absorption loss are necessary to fully substantiate this phenomenon. These calculations must consider all conditions leading to dielectric resonance in relatively thick layers of the studied TFC material. A comparative analysis of tabulated transmission loss values revealed that all samples exhibited presumably radio-transparency in the X-band. Of particular interest is the finding that the $(PVC)_{70}/(AC\text{-}H_2O_2)_{30}$ TFC sample with the highest AC-H_2O_2 concentration (30 wt.%) exhibited the most negative minimum, mean, and maximum transmission loss values of –1.5, –1.2, and –1.1 dB, respectively. These values indicate reduced microwave transmission through the composite.

In the production of TFCs, the addition of AC-H_2O_2 as PVC filler demonstrates the influence on the microwave properties of the resulting $(PVC)_{100-x}/(AC\text{-}H_2O_2)_x$ TFCs within the X-band (Table 2). Specifically, the mean reflection loss values differ by approximately 11 dB between $(PVC)_{99.8}/(AC\text{-}H_2O_2)_{0.2}$ TFCs and $(PVC)_{70}/(AC\text{-}H_2O_2)_{30}$ TFCs, which have the minimum and maximum AC-H_2O_2 filler concentrations, respectively. Experimental data show that transmission loss values of EMR within the X-band can be tuned to some extent at the preparation stage of these TFCs.

When evaluating the shielding properties of any composite material, it is important to examine the influence of filler concentration on interaction with EMR within a specific frequency range. It is also important to determine the effect of modification on filler properties, particularly compared to unmodified AC embedded in the same polymer matrix.

Many carbon materials, including carbon, carbon black, graphene, carbon nanotubes, and carbon spheres, are used as fillers in the formation of shielding material [21, 28, 39]. However, granular AC filler is the most convenient to work with in terms of chemical modification. In our previous work [41], we studied the microwave properties of a PVC-based composite with unmodified (pristine) AC. Comparing the data of [41] with the present work (Table 3), it can be concluded that the mean reflection loss values are higher for $(PVC)_{100-x}/(Filler)_x$ TFC samples when oxidized AC is used as a filler compared to the non-modified AC, especially at the filler concentration x above 10 wt.% (Fig. 10a, Table 3).

For high filler concentrations (x = 10…30 wt.%), the difference in the mean reflection loss values (Δ_r) between the $(PVC)_{100-x}/(Filler)_x$ TFC samples with AC-H_2O_2 and AC fillers ranges from –4.8 to –8.7 dB, with the maximum of –8.7 dB at a 20 wt.% filler concentration. These data suggest that oxidized AC is more effective at reflecting EMR within the X-band.

Comparing the transmission loss values of EMR through PVC-based composites with the unmodified AC and oxidized AC (AC-H_2O_2), one can see that the effect of the AC filler oxidative modification is less pronounced in this case than in the wave reflection regime (Fig. 10b, Table 3). This effect is negligible at low filler concentrations. The difference in the transmission loss values (Δ_t) between the AC-H_2O_2 and AC-containing $(PVC)_{100-x}/(Filler)_x$ TFCs is only noticeable at high filler concentrations (x > 20 wt.%). A maximum Δ_t of +0.4 dB is reached at an AC-H_2O_2 filler concentration x of 20 and 30 wt.%, but this Δ_t value can be considered insignificant.

Table 3. Mean reflection loss and mean transmission loss values of $(PVC)_{100-x}/(Filler)_x$ TFCs, where the filler is either AC-H_2O_2 or AC, and difference between them (Δ_r and Δ_t).

x, wt.%	Mean reflection loss values, dB		Difference	Mean transmission loss values, dB		Difference
	AC-H_2O_2	AC [41]	Δ_r	AC-H_2O_2	AC [41]	Δ_t
0.0	–22.8		–	–0.1		–
0.2	–21.7	–26.1	–4.4	–0.2	–0.2	0
0.5	–21.2	–25.6	–4.4	–0.2	–0.3	–0.1
1	–21.2	–25.5	–4.3	–0.3	–0.4	–0.1
5	–19.6	–23.0	–3.4	–0.3	–0.3	0
10	–17.7	–22.5	–4.8	–0.4	–0.3	+0.1
20	–14.5	–23.2	–8.7	–0.9	–0.5	+0.4
30	–11.8	–19.4	–7.6	–1.2	–0.8	+0.4

As a result of this study, $(PVC)_{100-x}/(AC\text{-}H_2O_2)_x$ TFCs were developed, and some of them remain radio-transparent within the X-band when filled with AC-H_2O_2, due to low mean transmission loss values. Studying the effect of the AC filler type on the microwave properties of the obtained composites showed that the reflected signal from the oxidized AC-based composite increases more intensively with increasing AC-H_2O_2 filler concentration than with the AC filler one. The mean reflection loss value varies depending on the AC-H_2O_2 filler content, indicating tunable reflective behavior. Specifically, increasing the concentration of oxidized AC (AC-H_2O_2), which is x in the $(PVC)_{100-x}/(AC\text{-}H_2O_2)_x$ TFCs, causes an increase in the intensity of the reflected signal as the reflection loss values become less negative, meaning more microwave energy is reflected. At the same time, the mean transmission loss values slightly decreased, as illustrated in Fig. 10b. This reduction was only clearly noticeable at higher filler concentrations (x >10 wt.%). In other words, transmission loss increased, meaning the numeric values became more negative (from –0.2 dB to –1.2 dB), indicating that less microwave energy was transmitted through the composites with the higher filler amount. At high filler concentrations in the $(PVC)_{100-x}/(Filler)_x$ TFCs, the slope of the transmission loss curve for composites containing oxidized AC is noticeably steeper than that for those containing unmodified AC. This trend suggests that the TFCs with oxidized AC absorb electromagnetic radiation more effectively, likely due to structural modifications introduced during oxidation. Oxidation of AC is presumed to cause significant changes in surface chemistry, porosity, and electronic structure, which in turn influence the interaction with electromagnetic fields and enhance dielectric loss mechanisms. To clarify the underlying mechanisms, further investigation is needed. Comparative studies using AC fillers with different degrees of oxidation are required to establish a direct correlation between structural transformations and the observed changes in transmission loss. These studies would provide insight into how the oxidation-induced structural evolution of the filler affects the electromagnetic performance of the PVC-based composites.

4. Conclusions

For the first time, thermally pressed TCFs were prepared using oxidized AC as the filler and PVC as the polymer matrix over a wide range of AC-H_2O_2 filler concentrations, specifically from 0.2 to 30 wt.%. The resulting films are 0.25-mm thick, flexible, and contain a carbon-based filler characterized by a developed porous structure and a large specific surface area. Oxidation of AC using a solution of H_2O_2 at the specified concentration is optimal for these filler samples, resulting in the best ratio of functional groups to specific surface area. SEM-EDX analysis shows that the oxygen concentration in the oxidized AC increases by 3.4 times compared to the unmodified AC sample. FTIR spectroscopy shows that the characteristic bands of PVC remain unchanged in the FTIR spectra of the TCFs, regardless of the carbon filler content. This minimal shift suggests that there is no significant chemical interaction between the PVC and the carbon filler within the TCFs. However, there may be some physical interactions, such as van der Waals bonding. Investigating the microwave properties of the manufactured TCFs, we suggested that TCFs with oxidized AC exhibited better electromagnetic field absorption. The oxidation process significantly alters the structure of the AC, which affects both microwave reflection and transmission behavior. Our experiments show that when oxidized AC is used as a filler in the PVC matrix, the reflection loss values increase more rapidly with filler concentration compared to unmodified AC, especially at x from 10 to 30 wt.%. A similar but decreasing trend is observed for the transmission loss values. Within the X-band, at the highest filler concentration of 30 wt.% in the $(PVC)_{100-x}/(Filler)_x$ TFCs, the difference in the reflection loss values Δ_r between oxidized AC and unmodified AC is –11.4 dB. The difference in the transmission loss values Δ_t is +0.4 dB. This variation of meaningful parameters opens tuning possibilities for further applications.

Acknowledgments

The authors are in debt to the Presidium of the National Academy of Sciences of Ukraine for the partial financing of the work. This work has been supported in part by the

Ministry of Education and Science of Ukraine: The Grant of the Ministry of Education and Science of Ukraine for the prospective development of a scientific direction "Mathematical sciences and natural sciences" at the Taras Shevchenko National University of Kyiv. The authors acknowledge the National Research Foundation of Ukraine (NRFU) and the "Excellent Science in Ukraine" program (Grant No. 2023.03/0193) for supporting morphological investigations. Authors are grateful for support from the Operational Program Integrated Infrastructure within the project "Environmental Engineering for a Healthy Environment", ITMS code: 313011T496, co-financed by the European Regional Development Fund.

References

1. Mikinka E., Siwak M. Recent advances in electromagnetic interference shielding properties of carbon-fibre-reinforced polymer composites – a topical review. *J. Mater. Sci.: Mater. Electron*. 2021. **32**. P. 24585–24643. https://doi.org/10.1007/s10854-021-06900-8.
2. Kim J.H., Lee J., Kim H. *et al*. Possible effects of radiofrequency electromagnetic field exposure on central nerve system. *Biomol. Ther.* 2019. **27**. P. 265–275. https://doi.org/10.4062/biomolther.2018.152.
3. Gunwant D., Vedrtnam A. Microwave absorbing properties of carbon fiber based materials: A review and prospective. *J. Alloys Compd*. 2021. **881**, No 10. P. 160572. https://doi.org/10.1016/j.jallcom.2021.160572.
4. Agarwal A., Desai N.R., Makker K. *et al.* Effects of radiofrequency electromagnetic waves (RF-EMW) from cellular phones on human ejaculated semen: an in vitro pilot study. *Fertil. Steril*. 2009. **92**. P. 1318–1325. https://doi.org/10.1016/j.fertnstert.2008.08.022.
5. Wu Y., Wang Z., Liu X. *et al.* Ultralight graphene foam/conductive polymer composites for exceptional electromagnetic interference shielding. *ACS Appl. Mater. Interfaces.* 2017. **9**, No 10. P. 9059–9069. https://doi.org/10.1021/acsami.7b01017.
6. Nosheen A., Hussain M.T., Khalid M. *et al.* Development of protective cotton textiles against biohazards and harmful UV radiation using eco-friendly novel fiber-reactive bioactive agent. *Process Saf. Environ. Prot*. 2022. **165.** P. 431–444. https://doi.org/10.1016/j.psep.2022.07.035.
7. Li C., Li D., Zhang L. *et al.* Boosted microwave absorption performance of transition metal doped TiN fibers at elevated temperature. *Nano Res.* 2023. **16**. P. 3570–3579. https://doi.org/10.1007/s12274-023-5398-3.
8. Liu P., Wang Y., Zhang G. *et al.* Hierarchical engineering of double-shelled nanotubes toward hetero-interfaces induced polarization and microscale magnetic interaction. *Adv. Funct. Mater.* 2022. **32**. P. 2202588. https://doi.org/10.1002/adfm.202202588.
9. Zhang F., Wang Q., Zhou T. *et al.* A multi-band binary radar absorbing metamaterial based on a 3D low-permittivity all-dielectric structure. *J. Alloy Compd.* 2020. **814**. P. 152300. https://doi.org/10.1016/j.jallcom.2019.152300.
10. Wang Q., Zhang F., Xiong Y. *et al.* Dual-band binary metamaterial absorber based low-permittivity all-dielectric resonance surface. *J. Electron. Mater.* 2019. **48**, No 2. P. 787–793. https://doi.org/10.1007/s11664-018-6796-2.
11. Akram S., Ashraf M., Javid A. *et al.* Recent advances in electromagnetic interference (EMI) shielding textiles: A comprehensive review. *Synth. Met*. 2023. **294**. P. 117305. https://doi.org/10.1016/j.synthmet.2023.117305.
12. Baltusnikaite-Guzaitien J., Varnaite-Zuravliova S. Textile based shielding materials, Chap. 10 in: *Advanced Materials for Electromagnetic Shielding: Fundamentals, Properties, and Applications*, Eds. Jaroszewski M., Thomas S., Rane A.V. Wiley, USA, 2018. https://doi.org/10.1002/9781119128625.ch10.
13. Zhou M., Zhang S., Zhang L. *et al.* Integration of MXene and polymer: Unlocking the full potential of multifunctional composites for electromagnetic interference shielding. *J. Mater. Sci. Technol*. 2025. **226**, No 10. P. 12–35. https://doi.org/10.1016/j.jmst.2024.12.011.
14. Guo H., Feng H., Liu T. *et al.* "Brick-mud" porous impregnated-segregated polymer composites with excellent electrical insulation, high thermal conductivity, and good electromagnetic interference shielding. *Polymer*. 2025. **316**. P. 127891. https://doi.org/10.1016/j.polymer.2024.127891.
15. Feng R., Zhu W., Yang W. *et al.* Scalable production of flexible and multifunctional graphene-based polymer composite film for high-performance electromagnetic interference shielding. *Carbon*. 2025. **233**. P. 119875. https://doi.org/10.1016/j.carbon.2024.119875.
16. Bheema R.K., Gopu J., Bhaskaran K. *et al.* A review on recent progress in polymer composites for effective electromagnetic interference shielding properties – structures, process, and sustainability approaches. *Nanoscale Adv*. 2024. **6**, No 23. P. 5773–5802. https://doi.org/10.1039/d4na00572d.
17. Permyakova N., Zheltonozhskaya T., Revko O. *et al*. Self-assembly and metalation of pH-sensitive double hydrophilic block copolymers with interacting polymer components. *Macromol. Symp*. 2012. **317–318**, No 1. P. 63–74. https://doi.org/10.1002/masy.201100079.
18. Pratap V., Soni A.K., Baskey H.B. *et al*. Electromagnetic and radar absorbing properties of γ-Fe_2O_3/$Ba_4Co_2Fe_{36}O_{60}$-epoxy polymeric composites for stealth applications. *Solid State Sci*. 2021. **113.** P. 106553. https://doi.org/10.1016/j.solidstatesciences.2021.106553.
19. Wu Y., Tan S., Zhao Y. *et al*. Broadband multispectral compatible absorbers for radar, infrared and visible stealth application. *Prog. Mat. Sci.* 2023. **135**. https://doi.org/10.1016/j.pmatsci.2023.101088.
20. Sankaran S., Deshmukh K., Ahamed M.B., Pasha S.K.K. Recent advances in electromagnetic interference shielding properties of metal and carbon filler

reinforced flexible polymer composites: A review. *Compos. – A.: Appl. Sci. Manuf.* 2018. **114**. P. 49–71. https://doi.org/10.1016/j.compositesa.2018.08.006.
21. Abbasi H., Antunes M., Velasco J.I. Recent advances in carbon-based polymer nanocomposites for electromagnetic interference shielding. *Prog. Mater. Sci*. 2019. **103**. P. 319–373. https://doi.org/10.1016/j.pmatsci.2019.02.003.
22. Stein A., Wang Z., Fierke M.A. Functionalization of porous carbon materials with designed pore architecture. *Adv. Mater.* 2009. **21**, No 3. P. 265–293. https://doi.org/10.1002/adma.200801492.
23. Nwigboji I.H., Ejembi J.I., Wang Z. *et al.* Microwave absorption properties of multiwalled carbon nanotube (outer diameter 20–30 nm)–epoxy composites from 1 to 26.5 GHz. *Diam. Relat. Mater.* 2015. **52**. P. 66–71. https://doi.org/10.1016/j.diamond.2014.12.008.
24. Zhang X., Qi S., Zhao Y. *et al.* Synthesis and microwave absorption properties of Fe@carbon fibers. *RSC Adv.* 2020. **10**. P. 32561–32568. https://doi.org/10.1039/d0ra03547e.
25. Diyuk V.E., Grishchenko L.N., Yatsimirskii V.K. Kinetics of the dehydration of 2-propanol on modified activated charcoal containing acid sites. *Theor. Exp. Chem.* 2008. **44**. P. 331–337. https://doi.org/10.1007/s11237-008-9046-5.
26. Grishchenko L., Tsapyuk G., Novichenko N.S. *et al.* Amination of brominated nanoporous activated carbon beads for the preparation of CO_2 adsorbents. *Mol. Cryst. Liq. Cryst.* 2020. **699**, No 1. P. 20–33. https://doi.org/10.1080/15421406.2020.1732535.
27. Zaderko A.N., Grishchenko L.M., Pontiroli D. *et al.* Enhancing the performance of carbon electrodes in supercapacitors through medium-temperature fluoroalkylation. *Appl. Nanosci.* 2022. **12**, No 3. P. 361–376. https://doi.org/10.1007/s13204-020-01651-0.
28. Kumar R., Sahoo S., Joanni E. *et al.* Recent progress on carbon-based composite materials for microwave electromagnetic interference shielding. *Carbon*. 2021. **177**. P. 304–331. https://doi.org/10.1016/j.carbon.2021.02.091.
29. Permyakova N.M., Zheltonozhskaya T.B., Beregova T.V. *et al.* Micellar nanocarriers for anticancer drug melanin. *Mol. Cryst. Liq. Cryst*. 2016. **640**, No 1. P. 122–133. https://doi.org/10.1080/15421406.2016.1257307.
30. Tang C., Cheng M., Lai C. *et al.* Recent progress in the applications of non-metal modified graphitic carbon nitride in photocatalysis. *Coord. Chem. Rev*. 2023. **474**. P. 214846. https://doi.org/10.1016/j.ccr.2022.214846.
31. Chen T. Chen S., Anushya G. *et al.* Electrochemical energy storage applications of functionalized carbon-based nanomaterials: An overview. *Int. J. Electrochem. Sci.* 2024. **19**, No 5. P. 100548. https://doi.org/10.1016/j.ijoes.2024.100548.
32. Dong S., Hu P., Li X. *et al.* $NiCo_2S_4$ nanosheets on 3D wood-derived carbon for microwave absorption. *Chem. Eng. J.* 2020. **398**. P. 125588. https://doi.org/10.1016/j.cej.2020.125588.
33. Wang H., Meng F., Li J. *et al.* Carbonized design of hierarchical porous carbon/Fe_3O_4@Fe derived from loofah sponge to achieve tunable high-performance microwave absorption. *ACS Sustain. Chem. Eng.* 2018. **6**, No 9. P. 11801–11810. https://doi.org/10.1021/acssuschemeng.8b02089.
34. Diyuk V.E., Zaderko A.N., Grishchenko L.M. *et al.* Surface chemistry of fluoroalkylated nanoporous activated carbons: XPS and ^{19}F NMR study. *Appl. Nanosci.* 2022. **12**, No 3. P. 637–650. https://doi.org/10.1007/s13204-021-01717-7.
35. Grishchenko L., Vakaliuk A., Diyuk V. *et al.* Functionalization of surface layer of nanoporous carbon fibers with bromine and amine functional groups. *2017 IEEE 7th Int. Conf. Nanomater. Appl. & Prop. (NAP)*. 2017. **1**. P. 01PCSI19-1-01PCSI19-6. https://doi.org/10.1109/NAP.2017.8190155.
36. Diyuk V.E. Zaderko A.N., Grishchenko L.M. *et al.* Preparation, texture and surface chemistry characterization of nanoporous-activated carbons co-doped with fluorine and chlorine. *Appl. Nanosci.* 2022. **12**, No 7. P. 2103–2116. https://doi.org/10.1007/s13204-022-02459-w.
37. Singh K., Baheti V. A comprehensive review on activated carbon fabrics: preparation, characterization, and applications in electromagnetic interference shielding and joule heating. *J. Anal. Appl. Pyrolysis*. 2024. **182**. P. 106689. https://doi.org/10.1016/j.jaap.2024.106689.
38. Liu Z., Wang Y., Liu C., Gao X. Study on the influence of carbon fiber paper modification on electromagnetic shielding performance and simulation. *Surf. Interf*. **44**. 2024. P. 103825. https://doi.org/10.1016/j.surfin.2023.103825.
39. Wu N., Hu Q., Wei R. *et al.* Review on the electromagnetic interference shielding properties of carbon based materials and their novel composites: Recent progress, challenges and prospects. *Carbon*. 2021. **176**. P. 88–105. https://doi.org/10.1016/j.carbon.2021.01.124.
40. Grishchenko L.M., Moiseienko V.A., Goriachko A.M. *et al.* Preparation and electromagnetic microwave absorption performances of sulfurated and oxidized polyacrylonitrile carbon fibers. *Mol. Cryst. Liq. Cryst*. 2023. **751**, No 1. P. 1–9. https://doi.org/10.1080/15421406.2022.2073045.
41. Grishchenko L.M., Zhytnyk D.O., Matushko I.P. *et al.* Facile preparation of polyvinyl chloride/ activated carbon thin-film composites and study of their microwave absorption at Ka-band frequencies. *Mol. Cryst. Liq. Cryst*. 2024. **768**, No 8. P. 139–149. https://doi.org/10.1080/15421406.2024.2348193.
42. Grishchenko L.M., Moiseienko V.A., Goriachko A.M. *et al.* Electromagnetic microwave absorption performances of plasma brominated carbon fibers. *2022 IEEE 41st Int. Conf. ELNANO.* 2022. **1**. P. 105–110. https://doi.org/10.1109/ELNANO54667.2022.9927037.
43. Grishchenko L.M., Moiseienko V.A., Goriachko A.M. *et al.* Electromagnetic interference shielding of carbon fibers oxidatively brominated in the

liquid-phase. *2022 IEEE 41st Int. Conf. ELNANO.* 2022. **1**. P. 99–104. https://doi.org/10.1109/ELNANO54667.2022.9927041.
44. Grishchenko L.M., Moiseienko V.A., Malyshev V.Yu. *et al.* Electromagnetic microwave absorption performances of aminated carbon fibers. *2022 IEEE 2nd Ukrfinian Microwave Week.* 2022. **1**. P. 73–78. https://doi.org/10.1109/UkrMW58013.2022.10037027.
45. Grishchenko L.M., Moiseienko V.A., Diyuk V.E. *et al.* Effect of chlorination with carbon tetrachloride on the interaction of carbon fibers with electromagnetic radiation in the ultrahigh-frequency band. *Appl. Nanosci*. 2023. **13**. P. 7203–7217. https://doi.org/10.1007/s13204-023-02892-5.
46. Salgado M.F., Abioye A.M., Junoh M.M. *et al.* Preparation of activated carbon from babassu endocarpunder microwave radiation by physical activation. *2nd Int. Tropical Renewable Energy Conf. (i-TREC) 2017 IOP Publishing IOP Conf. Series: Earth and Environmental Science.* 2017. **105**. P. 012116. https://doi.org/10.1088/1755-1315/105/1/012116.
47. Nagalakshmi T.V., Emmanuel K.A., Babu Ch.S. *et al.* Preparation of mesoporous activated carbon from Jackfruit PPI-1 waste and development of different surface functional groups. *ILCPA*. 2015. **54**. P. 189–200. https://doi.org/10.18052/www.scipress.com/ILCPA.54.189.

Authors and CV

Liudmyla M. Grishchenko, Sen. Res., CSc, Senior Researcher at the Department of Chemistry, Taras Shevchenko National University of Kyiv, the Institute of Engineering Thermophysics, NASU, and the Chuiko Institute of Surface Chemistry, NASU. Her scientific interests related to problems of physical chemistry related to nanomaterials, carbon materials, composite materials (hybrid carbon-polymer systems), and materials for electromagnetic shielding.
E-mail: liudmyla.grishchenko@gmail.com,
https://orcid.org/0000-0002-0342-4859

Vitaliy E. Diyuk, Assoc. Prof., CSc., Associate Professor at the Faculty of Chemistry, Taras Shevchenko National University of Kyiv, and a senior researcher at the Institute of Engineering Thermophysics, NASU. His scientific interests include thermal and porous properties of carbon materials and electromagnetic properties of composite materials based on them. E-mail: vdiyuk@gmail.com,
https://orcid.org/0000-0001-5183-5444

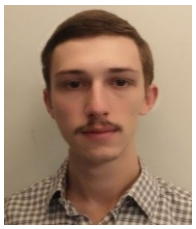

Dmytro O. Zhytnyk, PhD student at the Faculty of Radiophysics, Electronics and Computer Systems, Taras Shevchenko National University of Kyiv. His main activity is the study of composite materials (hybrid carbon-polymer systems) as materials for electromagnetic shielding.
E-mail: radiodima2000@gmail.com,
https://orcid.org/0009-0002-4106-4089

Igor P. Matushko, CSc., Senior Researcher at the Faculty of Physics, Taras Shevchenko National University of Kyiv. His main activity is the study of carbon materials and their physical properties.
E-mail: mipigor@gmail.com,
https://orcid.org/0000-0001-9643-6463

Yuriy V. Noskov, CSc., Senior Researcher at the Kukhar Institute of Bioorganic Chemistry and Petrochemistry, NASU. His main activity is the preparation and study of polymer thin film composites.
E-mail: yuriy.noskov@gmail.com,
https://orcid.org/0000-0002-4192-1733

Nataliia S. Novychenko, Junior Researcher at the Department of Electron Probe Research of Multifunctional Materials, Technical Center of NAS of Ukraine. Her scientific interests include SEM microscopy and EDX analysis.
E-mail: bilotka@gmail.com,
https://orcid.org/0000-0002-9971-0736

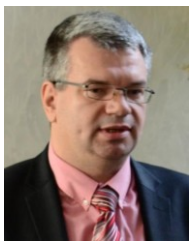

Ruslan T. Mariychuk, Assoc. Prof., CSc., Associate Professor at the Department of Ecology, Faculty of Humanities and Natural Sciences, University of Presov. IR spectroscopy, properties and characterization of biosorbents and green chemistry are the main areas of his activity.
E-mail: ruslan.mariychuk@unipo.sk,
https://orcid.org/0000-0001-8464-4142

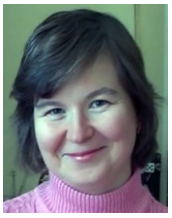

Olga Yu. Boldyrieva, Assoc. Prof., CSc., Associate Professor at the Faculty of Chemistry, Taras Shevchenko National University of Kyiv. The field of her scientific interests is physicochemical properties of solids.
E-mail: ob@univ.kiev.ua,
https://orcid.org/0000-0003-4756-3073

Mykola V. Makarets, Prof., DSc., is a Professor of the Theoretical Physics Chair, Faculty of Physics, Taras Shevchenko National University of Kyiv. His scientific interests include the interaction of fast ions and electrons with solids and nanostructures. E-mail: mmv@univ.kiev.ua, https://orcid.org/0009-0005-8329-4079

Oleksandr V. Mischanchuk, Junior Researcher at the Department of Quantum Chemistry and Chemical Physics of Nanosystems, Chuiko Institute of Surface Chemistry, NAS of Ukraine. The field of his scientific interest is TPD MS. E-mail: bigsnake@i.ua, https://orcid.org/0000-0001-6707-3341

Valerii V. Klepko, Prof., DSc., Head of the Molecular Physics Department at the Institute of Macromolecular Chemistry, NAS of Ukraine. The main areas of his work are phase transitions and critical phenomena in polymer systems, neutron spectroscopy of polymers, properties of molecules in "confined space" conditions. E-mail: vvklepko@ukr.net, https://orcid.org/0000-0001-8089-8305

Vladyslav V. Lisnyak, Sen. Res., DSc., Senior Researcher at the Institute of Macromolecular Chemistry and Chuiko Institute of Surface Chemistry, NASU, and a research professor at the Western Caspian University, Republic of Azerbaijan. His scientific interests include physical chemistry of carbon materials and special properties of thin film polymer composites. E-mail: lisnyak@nas.gov.ua, https://orcid.org/0000-0002-6820-1445

Authors' contributions

Grishchenko L.M.: project administration, investigation, visualization, writing – original draft.
Diyuk V.E.: resources, investigation, visualization, analysis, writing – review & editing.
Zhytnyk D.O.: investigation.
Matushko I.P.: investigation, visualization, writing – review & editing.
Novychenko N.S.: investigation.
Noskov Y.V.: investigation, sample preparation technology.
Mariychuk R.T.: investigation, writing – review & editing.
Boldyrieva O.Yu.: investigation.
Makarets M.V.: resources.
Klepko V.V.: resources.
Mischanchuk O.V.: investigation.
Lisnyak V.V.: formulation of the problem, formal analysis, data curation, writing – review & editing.

Властивості тонких композитних плівок полівінілхлорид/окислене активоване вугілля в X діапазоні мікрохвиль

Л.М. Гріщенко, В.Є. Діюк, Д.О. Житник, І.П. Матушко, Ю.В. Носков, Н.С. Новиченко, Р.Т. Марійчук, О.Ю. Болдирєва, М.В. Макарець, В.В. Клепко, О.В. Місчанчук, В.В. Лісняк

Анотація. З порошків полівінілхлориду (ПВХ) та окисненого активованого вугілля (АВ-H_2O_2) гарячим пресуванням формували тонкоплівкові композити (ТПК) складу $ПВХ_{100-x}/(АВ\text{-}H_2O_2)_x$, де x = 0,2…30% мас. Наноструктуру, морфологію та склад АВ-H_2O_2 досліджували за допомогою скануючої електронної мікроскопії та енергодисперсійної рентгенівської спектроскопії. Методами термічного аналізу оцінювали термостабільність поверхневих вуглець-кисневих груп наповнювача АВ-H_2O_2. Вплив вмісту АВ-H_2O_2 на електромагнітну прозорість ТПК $ПВХ_{100-x}/(АВ\text{-}H_2O_2)_x$ оцінювали на мікрохвильових частотах X-діапазону. Пропускання мікрохвиль виявило слабку залежність від концентрації наповнювача, тоді як втрати на відбиття змінювались у межах від –21,7 до –11,8 дБ при збільшенні x від 0,2 до 30% мас. Порівняння з аналогічними ТПК, що містили вихідне АВ, показало, що окиснення наповнювача суттєво впливає на властивості ТПК. Різниця у середніх значеннях втрат на відбиття між зразками $ПВХ_{100-x}/(АВ\text{-}H_2O_2)_x$ та $ПВХ_{100-x}/(АВ)_x$ коливалася від –3,4 дБ при x < 5% мас. до –8,7 дБ при x = 20–30% мас.

Ключові слова: тонкоплівкові композити, полі(вінілхлорид), активоване вугілля, окиснення, екранування електромагнітного випромінювання, відбиття мікрохвильового випромінювання.